

Article

An Optimal Model for Determination Shut-in Time Post-Hydraulic Fracturing of Shale Gas Wells: Model, Validation, and Application

Jianmin Li ¹, Gang Tian ¹, Xi Chen ¹, Bobo Xie ¹, Xin Zhang ¹, Jinchi Teng ¹, Zhihong Zhao ^{2,*} and Haozeng Jin ²

¹ PetroChina Xinjiang Oilfield Company, Karamay 834000, China; zy-ljm@petrochina.com.cn (J.L.); tgl2014@petrochina.com.cn (G.T.); chenxi@petrochina.com.cn (X.C.); xiebb@petrochina.com.cn (B.X.); gcyzhangxin@petrochina.com.cn (X.Z.); tengjinchi@petrochina.com.cn (J.T.)

² State Key Laboratory of Southwest Petroleum University, Chengdu 610500, China; jinhaozeng@gmail.com

* Correspondence: zhaozhong@swpu.edu.cn

Abstract: The global shale gas resources are huge and have good development prospects, but shale is mainly composed of nanoscale pores, which have the characteristics of low porosity and low permeability. Horizontal drilling and volume fracturing techniques have become the effective means for developing the shale reservoirs. However, a large amount of mining data indicate that the fracturing fluid trapped in the reservoir will inevitably cause hydration interaction between water and rock. On the one hand, the intrusion of fracturing fluid into the formation causes cracks to expand, which is conducive to the formation of complex fracture networks; on the other hand, the intrusion of fracturing fluid into the formation causes the volume expansion of clay minerals, resulting in liquid-phase trap damage. At present, the determination of well closure time is mainly based on experience without theoretical guidance. Therefore, how to effectively play the positive role of shale hydration while minimizing its negative effects is the key to optimizing the well closure time after fracturing. This paper first analyzes the shale pore characteristics of organic pores, clay pores, and brittle mineral pores, and the multi-pore self-absorption model of shale is established. Then, combined with the distribution characteristics of shale hydraulic fracturing fluid in the reservoir, the calculation model of backflow rate and shut-in time is established. Finally, the model is validated and applied with an experiment and example well. The research results show that the self-imbibition rate increases with the increase in self-imbibition time, and the flowback rate decreases with the increase in self-imbibition time. The self-imbibition of slick water is the maximum, the self-imbibition of breaking fluid is the minimum, and the self-imbibition of mixed fluid is the middle, and the backflow rates of these three liquids are in reverse order. It is recommended the shut-in time of Longmaxi Formation shale is 17 days according to the hydration and infiltration model.



Citation: Li, J.; Tian, G.; Chen, X.; Xie, B.; Zhang, X.; Teng, J.; Zhao, Z.; Jin, H. An Optimal Model for Determination Shut-in Time Post-Hydraulic Fracturing of Shale Gas Wells: Model, Validation, and Application. *Processes* **2024**, *12*, 399. <https://doi.org/10.3390/pr12020399>

Academic Editors: Dicho Stratiev and Qingbang Meng

Received: 17 January 2024

Revised: 4 February 2024

Accepted: 14 February 2024

Published: 17 February 2024



Copyright: © 2024 by the authors. Licensee MDPI, Basel, Switzerland. This article is an open access article distributed under the terms and conditions of the Creative Commons Attribution (CC BY) license (<https://creativecommons.org/licenses/by/4.0/>).

Keywords: shale; hydraulic fracturing; self-imbibition; flowback; shut-in time

1. Introduction

The characteristics of the pore space in shale rocks can be summarized as having various features in terms of the extremely narrow pore throat, low porosity, high compactness, large specific surface area, complex minerals and organic matter, multiple pores coexisting, and natural cracks and weakly cemented surface development [1–3]. Consequently, conventional depressurization methods cannot achieve commercial exploitation of shale gas. Nevertheless, massive hydraulic fracturing has become a key technology for commercial exploitation of shale gas [4–6], as the horizontal wells associated with massive hydraulic fracturing can connect natural cracks to allow the form of flow channels for shale gas [7–9] through the bulk volume of reservoirs near to the wells. Ten thousand cubic meters of water-based fracturing fluid can be injected into shale formations during hydraulic fracturing [10]. Because of the differences in geological characteristics, in crushed fracture areas, and in fracturing fluid performance, the

fracturing fluid in shale reservoirs typically has high flowback rate, as shown in Table 1 [11,12]. Currently, it is widely recognized that there is a negative correlation between gas production and flowback rate after hydraulic fracturing in shale [13–16].

Table 1. Flowback rate after fracturing in North America and China shale.

North America	Flowback Rate (%)	China	Flowback Rate (%)
Barnet/Marcelus [17]	50	Weiyuan	40.3
Horn River [18]	25~55	Yongchuan	34.3
Haynesville [17]	5	Changning	12.7
Eagle Ford [19]	<20	Fuling	3.9
Average in North America [20]	6~10	\	\

The control factors of low flowback rate of fracturing fluid primarily include spontaneous imbibition effect of shale [18,21,22], unstable displacement of gas–water two-phase and gravity differentiation in fracturing fractures [23,24], and fracturing fluid retention in secondary fractures [25]. The spontaneous imbibition effect is the major factor, which is different from the conventional reservoir post-hydraulic fracturing [26]. Imbibition is a process in which the porous medium spontaneously draws in wetting liquid under a capillary pressure drop [27]. In addition to the capillary force, the imbibition in the shale reservoir is also powered by the osmotic pressure [20,28].

The shale microstructure is complex and unique, especially when the clay content is high, which is when pores and bedding in clay are developed. The traditional perspective is that shale water absorption causes an increase in the water saturation, the clay expands to fill the pores, and the permeability reduces in both matrix and fractures [29–31]. However, recent studies have suggested that the swelling of the shale, the increase in the pore pressure, and the weakening in mechanical strength of the rock can induce the micro-crack initiation, consequently improving the permeability of shale [1,13,29,32,33].

As shale imbibition can increase reservoir permeability, many researchers have studied the effect of well shut-in on yield. They found that well shut-in can enhance shale imbibition, which is favorable for the reduction in water saturation in the fractures, meaning it can increase the initial production, but has no significant impact on long-term production [13,14]. Simulating the effects of phase infiltration, capillary force, and effective stress on well shut-in reveals that wells should be shut-in right after fracturing and kept for a long period of time [34]. Well shut-in can increase gas and reduce water production; unfortunately this effect does not last quite long [35]. According to the previous studies, well shut-in can increase the production at early stage and for a short period. In practice, however, the shut-in time after a hydraulic fracturing has a lack of theoretical interpretation but just experimental understanding.

Due to the significant differences in pore shape, pore size, pore genesis, and wettability among organic pores, brittle mineral pores, and clay pores, the imbibition depth and imbibition amount of the three types of pores are significantly different. This article focuses on the mechanism of imbibing water for shale, and conducts research from the aspects of shale microstructure characteristics and imbibition force, establishing three imbibition models for three types of pores, i.e., organic pores, brittle mineral pores, and clay pores. A model is then introduced for calculating the shale shut-in time by combining with the direction of fracturing fluid flow during shale fracturing, which is validated by comparing with experimental data.

2. Shale Multiple-Pore Imbibition Model

Shale rock is a multi-porous medium; the pore type includes the organic pores, clay pores, and brittle mineral pores, and because the origins of the different types of the pores are different, the pore size, shape (Figure 1), and the distribution of the pore size have significant differences (Figure 2).

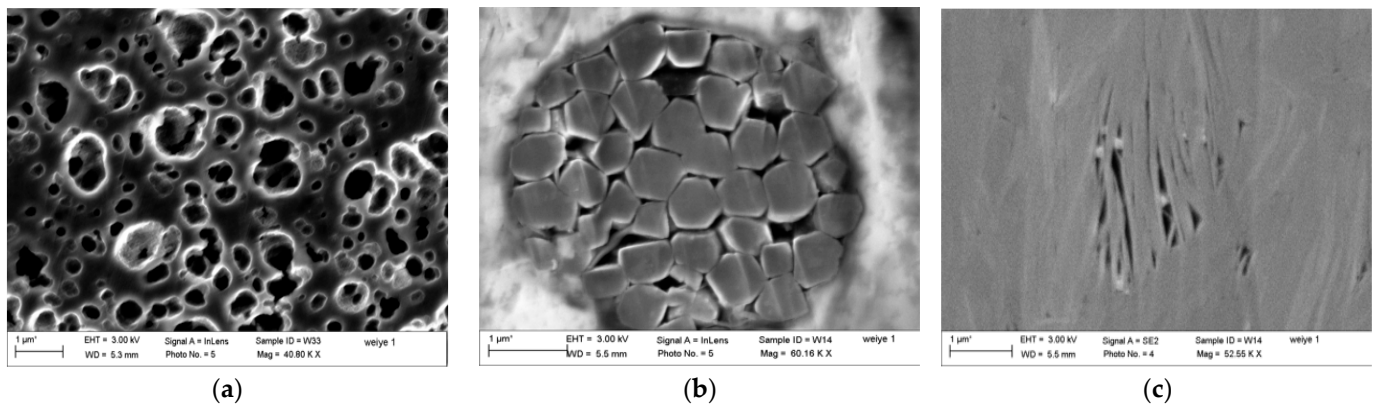


Figure 1. Types of pores in shale. (a) Organic pores, (b) brittle mineral pores, (c) clay pores.

Yuman et al. (2015) stated that the pores of shale can be subdivided into the clay pores, brittle mineral pores, and organic pore, as expressed in Equation (1) [36]. Based on the assumption, shale imbibition can then be decomposed into three types of pore imbibition for organic pores, brittle mineral pores, and clay pores. However, the forces of imbibition for three types of pores are different during the process of the imbibition. Thus, we establish the shale multi-pore imbibition model based on the force of the imbibition for three types of pores.

$$\phi = \phi_{fb} + \phi_{fc} + \phi_{fo} \quad (1)$$

where ϕ is the total porosity (%) of shale, and ϕ_{fb} , ϕ_{fc} , and ϕ_{fo} are the porosities accounting for brittle mineral pores, clay pores, and organic pores, respectively.

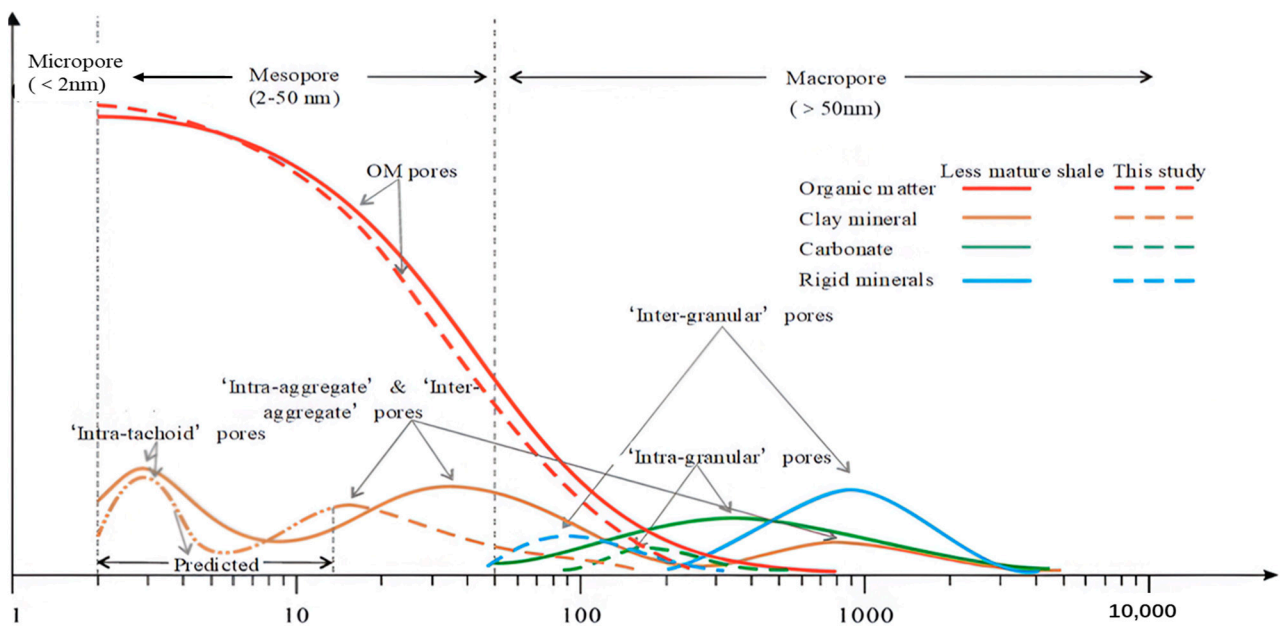


Figure 2. The relationship between pore size and type [37,38].

2.1. Pore Imbibition Models

(1) Organic pores and brittle pores

It can be seen from Figure 2 that the pore shape of organic pores and brittle minerals is similar to an ellipse, so the elliptical capillary fractal imbibition model can be used to describe the imbibition in these pores. There are no significant differences in the microstructure and physical property parameters for the organic pores and brittle pores. Under the condition of ignoring the influence of gravity on the imbibition of the water phase, the

imbibition effect of the organic pores and brittle mineral pores is only controlled by the force of the capillary. Therefore, we have the same imbibition models for ease of calculation, as shown in Equation (2) [39].

$$L_e = \left\langle \frac{\sigma \cos \theta b_{max}^{D_f-2} (m+1) (2-D_f) (b_{max} - b_{min})}{8\mu D_f b_{min}^{1-D_T} (1-\phi)} \sum_{k=0}^n \omega_k \left\{ \frac{b_k^{D_T-D_f} [mk_b^2 + 6(m+1)L_s b_k + 32L_s]}{(m^2+1)k_b + 4(m+1)L_s} \right\} \right\rangle^{\frac{1}{2D_T}} \cdot t^{\frac{1}{2D_T}} \quad (2)$$

$$b_k = \frac{b_{max} - b_{min}}{2} t_k + \frac{b_{max} + b_{min}}{2} \quad (3)$$

where σ is interfacial tension between two phases, mN/m; ϕ porosity, %; θ is wetting contact angle, °; D_f is fractal dimension; D_T is flexibility fractal dimension; b_{min} is minimum pore diameter, nm; b_{max} is maximum pore diameter, nm; μ is aqueous phase viscosity, mPa·s; L_s boundary slip length, nm; t is imbibition time, min; m is aspect ratio of elliptical pores; n is the number of interval segments; ω_k is weight coefficient; and t_k is Gaussian point determined by n .

If a four-point formula is chosen, $t_k = \pm 0.8611363, \pm 0.3399810, \omega_k = 0.3478548, 0.6521452$.

(2) Clay minerals pores

It can be seen from Figure 2 that the shape of the clay pores is significantly different from the shapes of the organic and brittle pores. The clay pores exhibit a slender shape. Therefore, the model of the parallel fracture can be used to describe the imbibition phenomenon in these pores. Moreover, the force of imbibition for the clay pores is significantly different from the forces of imbibition of the organic pores and brittle mineral pores. It is not only affected by the capillary force, but also by the osmotic pressure. In the effective imbibition flow range of the reservoir, the influence of the gravity on the imbibition is very small compared with the capillary force and the osmotic pressure, because the 10-m high water column produces a gravity of 0.1 MPa, meaning the influence of the gravity can be ignored. The fractal model of clay pore imbibition length (L_c) is expressed as follows:

$$L_c = \left\{ \frac{(D_{Tc} + D_{fc} - 1)(2 - D_{fc})}{D_{fc} w_{min}^{1-D_{Tc}} (1 - \phi)} \left[\frac{\sigma \cos \theta_c}{3\mu} (A_2 + 6L_{sc} B_2) + \frac{p_\pi}{6\mu} (C_2 + 6L_{sc} A_2) \right] \right\}^{\frac{1}{2D_{Tc}}} \cdot t^{\frac{1}{2D_{Tc}}}, \quad (4)$$

$$A_2 = \frac{w_{max}^{D_{Tc}} (1 - \beta_c^{2+D_{Tc}-D_{fc}})}{2 + D_{Tc} - D_{fc}}; B_2 = \frac{w_{max}^{D_{Tc}-1} (1 - \beta_c^{1+D_{Tc}-D_{fc}})}{1 + D_{Tc} - D_{fc}}; C_2 = \frac{w_{max}^{1+D_{Tc}} (1 - \beta_c^{1+D_{Tc}-D_{fc}})}{3 + D_{Tc} - D_{fc}}; \beta_c = \frac{w_{min}}{w_{max}} \quad (5)$$

where w_{max} is the maximum clay pore width, nm; w_{min} is the minimum clay pore width, nm; subscripts c represents clay pore; and p_π is osmotic pressure, and can be expressed by [40]:

$$p_\pi = \varepsilon E_\pi RT (C_{sh} - C_f) \quad (6)$$

where R is a gas constant of 0.08206 (L·KPa)/(mol·K), usually; T is temperature of formation, K; C_{sh} is molar concentration of solute in the original formation water, mol/L; C_f is molar concentration of solute in fracturing fluid, mol/L; ε is number of ions after solute ionization (example.g., NaCl value is 2); and E_π is membrane efficiency, and can be expressed as follows [40]:

$$E_\pi = 1 - \frac{(R_{ca-w} + 1)C_a/C_s}{\{R_{ca-w}(C_a/C_c) + 1 + R_{a-mw}[R_{ca-m}(C_a/C_c) + 1]\}\phi_c} \quad (7)$$

$$\begin{cases} C_s = \frac{1}{2}(C_f + C_{sh}) \approx \frac{1}{2}C_{sh} \\ C_a = -\frac{1}{2}E_{CEC}\rho_{clay}(1 - \phi_c) + \frac{1}{2}\left[E_{CEC}^2\rho_{clay}^2(1 - \phi_c)^2 + 4C_s^2\phi_c^2\right]^{\frac{1}{2}} \\ C_c = C_a + E_{CEC}\rho_{clay}(1 - \phi_c) \end{cases} \quad (8)$$

where C_s is arithmetic mean of solute in solution on both sides of semi-permeable membrane; C_a is the concentration of anions in the pores of the semi-permeable membrane; E_{CEC} is the cation exchange capacity of shale; ρ_{clay} is the density of clay minerals; R_{ca-m} is ratio of friction coefficient of anions to water; R_{ca-w} is the ratio of the friction coefficient of the anions to the membrane; and R_{a-mw} is the ratio of anion–semi-permeable membrane to cation–water friction coefficient.

(3) Multiple pore self-imbibition model

According to the shale multi-porosity splitting model [36], the total porosity of shale can be decomposed into organic porosity (ϕ_{to}), brittle mineral porosity (ϕ_{tb}), and clay porosity (ϕ_{tc}). The cumulative imbibition volume V_{im} is, thus, the sum of the volumes imbibed from organic pores, brittle mineral pores, and clay pores. The shale imbibition model of multiple pores can be expressed as:

$$V_{im} = V_{imo} + V_{imb} + V_{imc} = A_f\phi_{to}L_o + A_f\phi_{tb}L_b + A_f\phi_{tc}L_c \quad (9)$$

where V_{im} is total imbibition volume, m^3 ; V_{imo} , V_{imb} , V_{imc} are imbibition volume of organic pores, clay pores, and brittle mineral pores, m^3 , respectively; and A_f is contact area of fracturing fluid and shale, m^2 , which can be obtained using the pressure drop analysis method in Equation (10).

$$A_f = 2\frac{V_{inj} - V_{leak}}{w_f} \quad (10)$$

where V_{leak} is the fluid loss volume, m^3 , which can be obtained from pressure drop data [41]; V_{inj} is the volume injection fracturing fluid, shale reservoir filtration typically accounts for 10–40%, the Horn River shale is estimated at 30% [42]; and w_f is the average fracture width, which can be determined with pressure drop analysis method of Equation (11) [42].

$$f(w_f) = \frac{C_f^2 L_m}{2DC_{sh}\Delta t} \frac{dN_w}{dC_f}, \quad (11)$$

where Δt is the backflow curve discrete element time; N_w is non-dimensional backflow of fracturing fluid after fracturing (the ratio of the amount of phased reflux to the amount of cumulative reflux).

According to Equation (11), the average fracture width can be obtained, and the fracture area of each section can be calculated according to Equation (10).

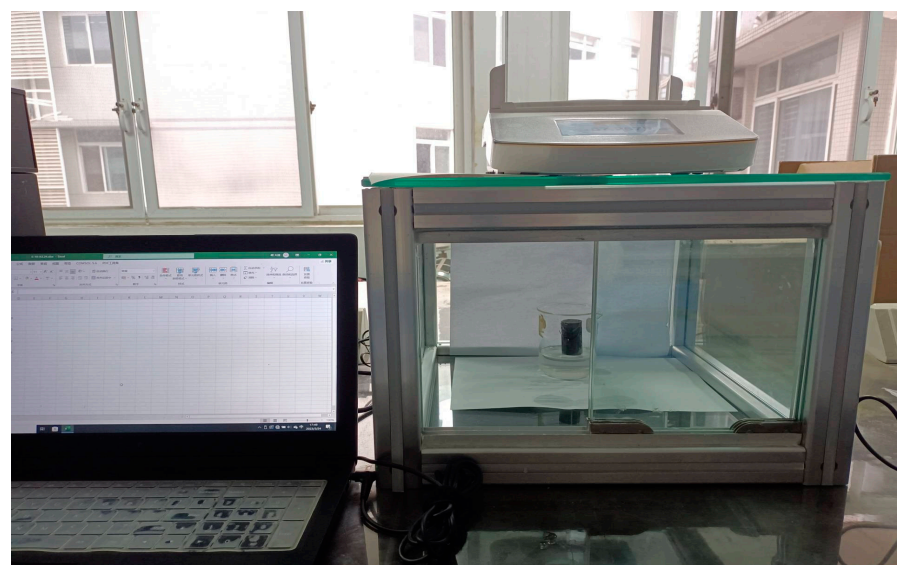
2.2. Validation and Analysis

Experimental materials:

A shale core of the Longmaxi Formation in Sichuan Basin was chosen and the imbibed fluid is distilled water. Other physical and chemical properties of the experimental materials are shown in Table 2. In order to improve the accuracy of the data, the analytical scale automatically weighs and measures. The range of the analytical scale is 220 g, and the precision is 0.0001 g. The experimental setup is shown in Figure 3.

Table 2. Shale sample and fluid essential parameters.

Parameters	Value		
	Organic Pore	Brittle Pore	Clay Pore
Wetting contact angle θ ($^{\circ}$)	80.40	16.20	11.50
Mineral porosity (%)	20.08	0.88	7.84
Aspect ratio of elliptical pores m (dimensionless)	2.336	3.286	\
Boundary slip length L_s (nm)	4.41	1.56	1.53
Maximum pore diameter b_{\max} (nm)	627	1020	461
Minimum pore diameter b_{\min} (nm)	1.47	7.5	1.47
Fractal dimension D_f	2.681	2.549	2.619
Flexibility fractal dimension D_T	1.212	1.297	1.255
The porosity of the core $\phi_{to}/\phi_{tb}/\phi_{tc}$ (%)	1.534	0.676	1.600
Water–core contact area A_f (cm 2)		6.45	
Viscosity of water μ (mPa·s)		1.00	
Gas–water interfacial tension σ (mN/m)		74.10	
Molar concentration of solute in the original formation water C_{sh} (mol/L)		0.525	
Molar concentration of solute in fracturing fluid C_f (mol/L)		0.017	
Test temperature T (K)		293.15	
The cation exchange capacity of shale E_{CEC}		3.7	
Ratio of friction coefficient between anions and water R_{ca-m}		1.8	
The ratio of the friction coefficient between the anions and the membrane R_{ca-w}		1.63	
The ratio of anion–semi-permeable membrane to cation–water friction coefficient R_{a-mw}		1.37	

**Figure 3.** Schematic diagram of the forward imbibition experimental setup.

Experimental procedures:

- (1) Prepare a standard shale core of 5.0 cm in length and measure the basic parameters of the core and fluid. The test results are shown in Table 2;
- (2) Dry the core by placing the core in an oven for more than 10 h, to weigh, and to wrap the core surface with a heat shrinkable tube, as shown in Figure 3;
- (3) Monitor the change in imbibition weight over time using a scale, and carry out the same drying treatment in the end of the experiment.

It can be seen from Figure 4 that the calculation results are close to the experimental results, which proves that the imbibition model is accurate and reliable. When the shale imbibes for 70 min, the imbibition volume increases first and then decreases with the imbibition time passing. We can find that test results are 10~20% higher than calculation results in the second stage because the induced fractures promote shale imbibition (Figure 4). In the third stage, test results are lower than the calculated results due to core size effect and shale tending to be saturated resulting in reduced imbibition speed. Shale imbibition is a coupling process between liquid-phase flow and the dynamic change in shale microstructure; by contrast, the microstructure of traditional tight sandstone does not change during the imbibition process. In this work, we mainly study the imbibition in shale multi-porosity microstructures, and the dynamic changes in microscopic structure are not considered in the multiple-pore imbibition model.

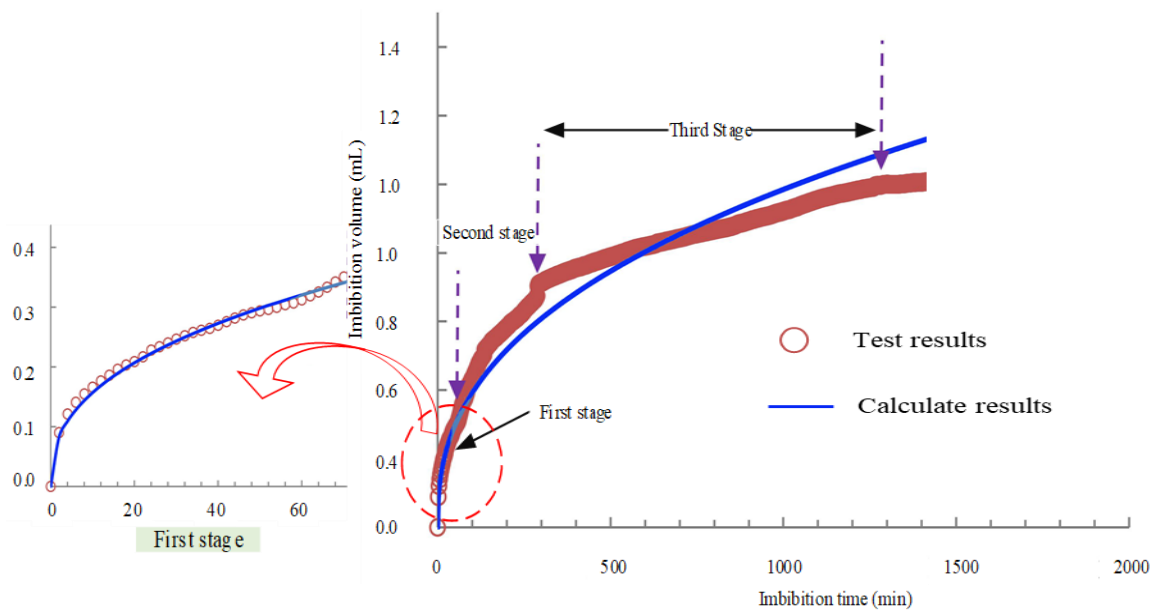


Figure 4. Comparison of calculation with experimental results.

3. Determination of Shut-In Time Model

Shale gas horizontal well staged fracturing has the characteristics of more fracturing segments and longer operation time. This results in a larger time interval between the end and toe fracturing segments, and the imbibition volume calculation needs to take into account the time difference. The imbibition process during fracturing can be divided into two steps/periods. The first step is operation, when the imbibition time of various segments is distinct. The second step is well shut-in, during which all segments have the same imbibition time. During the operation stage, each segment is separated by the bridge plug. Therefore, the imbibition of each segment is independent, and the total imbibition volume during operation stage (V_{im1}) can be expressed as follows:

$$V_{im1} = \sum_{i=1}^n V_{imf,i} = \sum_{i=1}^n A_f \left(\phi_{to} C_{imo} t_{f,i}^{m_o} + \phi_{tb} C_{imb} t_{f,i}^{m_b} + \phi_{tc} C_{imc} t_{f,i}^{m_c} \right) \quad (12)$$

During the shut-in well stage, the bridge plug between the segments has been drilled through, thus, the imbibition volume can be given by:

$$V_{im2} = nA_f(\phi_{to}C_{imo} + \phi_{tb}C_{imb} + \phi_{tc}C_{imc})t_{shut} \quad (13)$$

where $V_{imf,i}$, V_{im1} , V_{im2} are the imbibition volume contributed by the I segment during the operation stage, the total imbibition volume during the operation, and the total imbibition volume of the shut-in stage, m^3 ; $t_{f,i}$ is imbibition time of operation the i , s ; t_{shut} is shut-in time, s ; n is the total fracturing segments of whole well. C_{imo} , C_{imb} , C_{imc} are the coefficients of Equations (2), (3), and (5), and they are expressed as follows:

$$C_{imo} = \left\langle \frac{\sigma \cos \theta_o b_{\max o}^{D_{fo}-2} (m_o + 1)(2 - D_{fo})(D_{To} + D_{fo} - 1)(b_{\max o} - b_{\min o})}{8\mu D_{fo} b_{\min o}^{1-D_{To}} (1 - \phi)} \sum_{k=0}^n \omega_k \left\{ \frac{b_{ko}^{D_{To}-D_{fo}} [m_o b_{ko}^2 + 6(m_o + 1)L_{so} b_{ko} + 32L_{so}^2]}{(m_o^2 + 1)b_{ko} + 4(m_o + 1)L_s} \right\} \right\rangle^{\frac{1}{2D_{To}}} \quad (14)$$

$$C_{imb} = \left\langle \frac{\sigma \cos \theta_b b_{\max b}^{D_{fb}-2} (m_b + 1)(2 - D_{fb})(D_{Tb} + D_{fb} - 1)(b_{\max b} - b_{\min b})}{8\mu D_{fb} b_{\min b}^{1-D_{Tb}} (1 - \phi)} \sum_{k=0}^n \omega_k \left\{ \frac{b_{kb}^{D_{Tb}-D_{fb}} [m_b b_{kb}^2 + 6(m_b + 1)L_{sb} b_{kb} + 32L_{sb}^2]}{(m_b^2 + 1)b_{kb} + 4(m_b + 1)L_s} \right\} \right\rangle^{\frac{1}{2D_{Tb}}} \quad (15)$$

$$C_{imc} = \left\{ \frac{(D_{Tc} + D_{fc} - 1)(2 - D_{fc})}{D_{fc} \omega_{\min}^{1-D_{Tc}} (1 - \phi)} \left[\frac{\sigma \cos \theta_c}{3\mu} (A_2 + 6L_{sc} B_2) + \frac{p\pi}{6\mu} (C_2 + 6L_{sc} A_2) \right] \right\}^{\frac{1}{2D_{Tc}}} \quad (16)$$

The imbibition rate is defined as the ratio of the imbibition volume to the volume of liquid that effectively creates the fractures. The expression is as follows:

$$N_{loss} = \frac{V_{im}}{V_{inj} - V_{leak}} \quad (17)$$

Suppose that the water phase is in a bound state after self-imbibition and there is no discharge, the expression of fracturing fluid backflow rate is as follows:

$$N_{fb} = \frac{V_{inj} - V_{im}}{V_{inj}} \quad (18)$$

When then imbibition rate reaches 100%, it indicates that the fracturing fluid in the fractures is completely imbibed into the shale matrix. At this time, there is no fracturing fluid remaining in the fractures, and there is no two-phase flow in the crack during production to reduce the permeability of crack [13,14]. The imbibition time of water phase minus the fracturing operation time is the shut-in time.

$$t_{shut} = \frac{V_{inj} - V_{leak} - V_{im1}}{nA_f(\phi_{to}C_{imo} + \phi_{tb}C_{imb} + \phi_{tc}C_{imc})} \quad (19)$$

4. Model Application Analysis

(1) Basic parameters of reservoir and fracturing

Take a well, named as W1, of the shale reservoir in Sichuan Basin as an example. Table 2 lists basic formation parameters while Table 3 reveals fracturing parameters. The main ionic composition of the backflow solution is NaCl, so the value of the ionic diffusion coefficient of the backflow solution approximate is $1.484 \times 10^{-9} \text{ m}^2/\text{s}$ [15]. The fracturing liquid properties of sliding water, breaking fluid, and linear glue are shown in Table 4.

Table 3. Fracturing parameters.

Parameters	Value	Parameters	Value
Fracturing segments	16	Fracturing time t (d)	16
Injection fluid volume V_{inj} (m ³)	27,740	Average fluid volume per segment V_{injfr} (m ³)	1733.75
Slippage and linear gel ratio	7: 3	Matrix Cl- salinity	15,291.8
Discrete element time Δt (d)	1	Diffusion coefficient (m ² /s)	1.484×10^{-9}

Table 4. Performance parameters of different types of liquids.

Liquid Type	Contact Angle (°)	Viscosity (mPa·s)	Surface Tension (mN/m)	Salinity (mol/L)	Density (g/cm ³)
Slick water	42.4	7	35.34	0	1
Breaking fluid	42.8	14	25.32	0	1.004

(2) Shut-in time calculation

Figure 5 shows the backflow rate under different self-imbibition rate and time with different fracturing fluid; it reveals that increasing the shut-in time, namely, increasing the self-imbibition time, causes a rise in the self-imbibition rate at the beginning and when decreasing the flowback rate thereafter, the self-imbibition of slick water reaches to its maximum, meanwhile the self-imbibition of breaking fluid achieves its minimum, and, furthermore, the self-imbibition of mixed fluid (the ratio of slick water to linear glue is 7:3) arrive at the middle. The backflow rates of these three liquids are in reverse order.

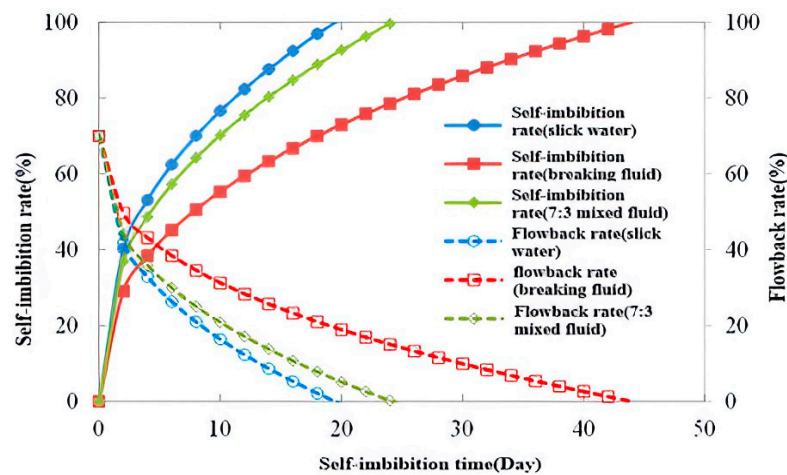


Figure 5. Backflow rate under different self-imbibition rate and time with different fracturing fluid.

Figure 6 is the self-absorption of each fracturing section during fracturing operation. The total self-imbibition is 7811.7 m³ with a total inject fluid of 27,740 m³, so the average self-imbibition fluid is 488.23 m³ per single stage during the shut-in time; in other words, the needed self-imbibition rate is 85.4%. According to Figure 4 or Equation (19), the shut-in time can be determined to be 17 days.

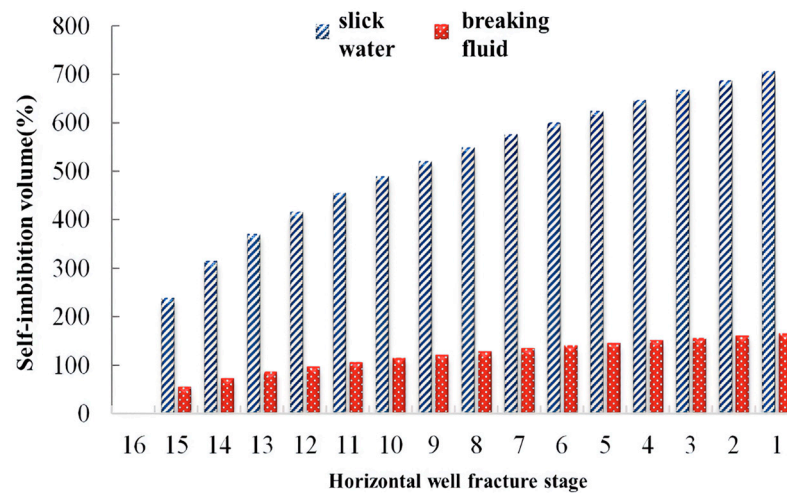


Figure 6. The self-absorption of each fracturing section during fracturing operation.

(3) Analysis of the flowback fluid data

Well W1 was actually closed for 7 days after fracturing operation, and then flowback was performed. According to the time of chlorine balance in the flowback fluid, the initial equilibrium of W1 was reached in 17–18 days, which was consistent with the calculated results by the proposed model. However, the shut-in of W1 lasted for 70 days, and after the long-time shut-in, the concentration of chlorine increased significantly (Figure 7). This indicates that ion exchange between fracturing fluid and formation fluid and the dissolution of shale matrix are still taking place during the shut-in after the initial equilibrium.

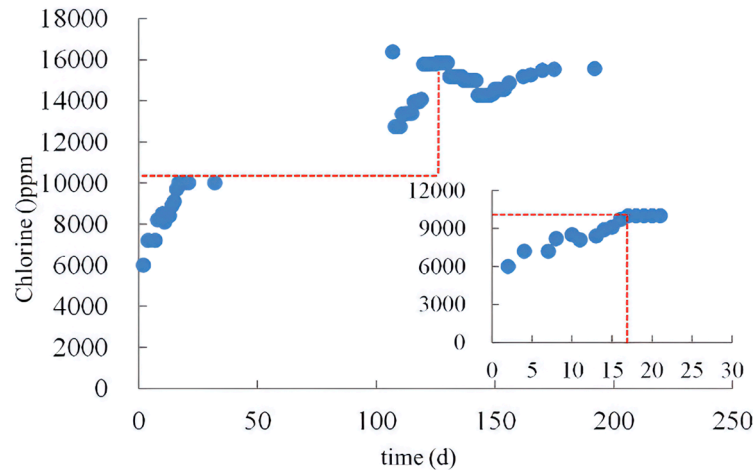


Figure 7. Backflow fluid curve in Well W1. The blue dots represent the recorded experimental data, while the red dashed line has no practical significance.

(4) Production dynamic analysis

From the production dynamic curve during the flowback process (Figure 8), it can be seen that the production of the water decreases rapidly after well W1 is shut-in, the trend of decrease is almost vertical, the production of the water almost decreases to 0 in a short period of time, indicating that the shut-in process increases the time of the imbibition. This results in a significant increase in cumulative imbibition. After 70 days, the W1 still produced a certain degree of water, and it indicates that the ability of displacing oil is limited and only relies on the imbibition, and other methods of increasing the production need to be combined to improve the production of the well.

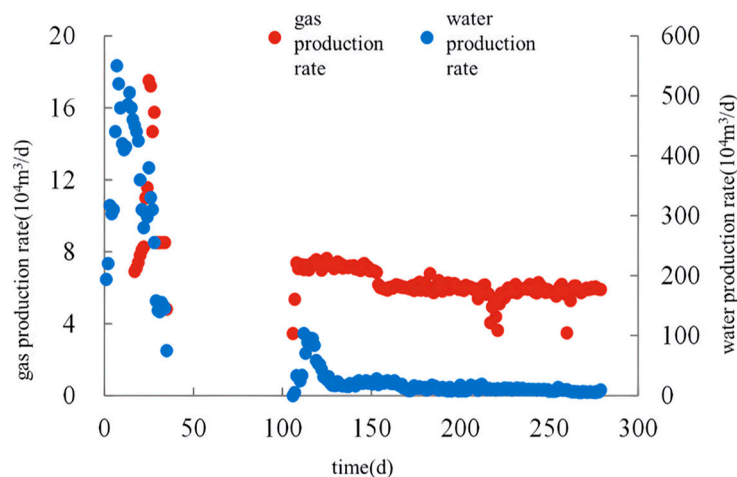


Figure 8. Production dynamic curve during flowback.

5. Conclusions

- (1) This article establishes a shale multi-pore imbibition model based on the assumption that the shale pores can be divided into the organic pores, brittle mineral pores, and the clay pores. The model can effectively simulate the early spontaneous infiltration and absorption process of shale;
- (2) The volume of the imbibition gradually increases with the hydration time: slick water > mixed liquid > gel-breaking liquid, while the infiltration rate gradually decreases. During the backflow process, the backflow rate and water imbibition of the three liquids show an opposite trend;
- (3) According to the self-imbibition of each fracturing period during fracturing operation, the total self-imbibition amount is 7811.7 m^3 with a total inject fluid volume of $27,740 \text{ m}^3$, so the average self-imbibition fluid volume is 488.23 m^3 per single stage during the shut-in time. According to the shale multi-pore self-imbibition model established in this article, the shut-in time can be determined to be 17 days;
- (4) According to the flowback data, the concentration of the chloride ions in the flowback fluid reaches initial equilibrium within 17–18 days, which is consistent with the results of the model calculation. However, the closure time of W1 lasted for 70 days, and the prolonged closure significantly increases the concentration of the chloride ions in the flowback fluid, indicating that there is still exchange of the ions between the fracturing fluid and the formation fluid during the initial ion equilibrium process of the shut-in;
- (5) It can be seen from the field production data that after the water productivity of W1 decreases rapidly, the trend of the declining is almost vertical. The production of the water almost decreases to 0 in a short period of the time, indicating that the process of the shut-in increases the time for imbibition. This leads to a significant increase in cumulative imbibition. After 70 days, well W1 still produced a certain amount of the water, indicating that the ability of displacing oil is limited and relies only on the imbibition. Other methods for increasing the production need to be combined to achieve this.

Author Contributions: Conceptualization, J.L., G.T., X.C., B.X., X.Z. and J.T.; Methodology, validation, investigation and writing, Z.Z. and H.J. All authors have read and agreed to the published version of the manuscript.

Funding: National Natural Science Foundation of China (project No. 51525404).

Data Availability Statement: Data are contained within the article.

Acknowledgments: The authors would like to acknowledge that this work was successfully completed through the financial support by the National Natural Science Foundation of China (project No. 51525404).

Conflicts of Interest: Authors J.L., G.T., X.C., B.X., X.Z. and J.T. were employed by the company PetroChina Xinjiang Oilfield Company. The remaining authors declare that the research was conducted in the absence of any commercial or financial relationships that could be construed as potential conflicts of interest.

References

1. Yuan, B.; Wang, Y.; Wei, N. The effects of fracturing fluid retention on permeability of shale reservoirs. *Energy Procedia* **2019**, *158*, 5934–5939. [[CrossRef](#)]
2. Yuan, B.; Wang, Y.; Zeng, S. Effect of Slick Water on Permeability of Shale Gas Reservoirs. *J. Energy Resour. Technol.* **2018**, *140*, 112901–112907. [[CrossRef](#)]
3. Zhang, S.; Xian, X.; Zhou, J.; Liu, G.; Guo, Y.; Zhao, Y.; Lu, Z. Experimental study of the pore structure characterization in shale with different particle size. *J. Energy Resour. Technol.* **2018**, *140*, 54502–54511. [[CrossRef](#)]
4. Ahn, C.H.; Dilmore, R.; Wang, J.Y. Modeling of hydraulic fracture propagation in shale gas reservoirs: A three-dimensional, two-phase model. *J. Energy Resour. Technol.* **2017**, *139*, 2903–2912. [[CrossRef](#)]
5. Guo, T.; Li, Y.; Ding, Y.; Qu, Z.; Gai, N.; Rui, Z. Evaluation of Acid Fracturing Treatments in Shale Formation. *Energy Fuels* **2017**, *31*, 10479–10489. [[CrossRef](#)]
6. Vincent, M.C. The next opportunity to improve hydraulic-fracture stimulation. *J. Petrol. Technol.* **2012**, *64*, 118–127. [[CrossRef](#)]
7. He, Y.; Cheng, S.; Li, S.; Huang, Y.; Qin, J.; Hu, L.; Yu, H. A semianalytical methodology to diagnose the locations of underperforming hydraulic fractures through pressure-transient analysis in tight gas reservoir. *SPE J.* **2017**, *22*, 924–939. [[CrossRef](#)]
8. Nasriani, H.R.; Jamiolahmady, M. Flowback cleanup mechanisms of post-hydraulic fracturing in unconventional natural gas reservoirs. *J. Nat. Gas Sci. Eng.* **2019**, *66*, 316–342. [[CrossRef](#)]
9. Sun, J.; David, S. Investigating the effect of improved fracture conductivity on production performance of hydraulic fractured wells through field case studies and numerical simulations. *J. Can. Pet. Technol.* **2015**, *54*, 442–449. [[CrossRef](#)]
10. Hull, N.M.; Rosenblum, J.S.; Robertson, C.E.; Harris, J.K.; Linden, K.G. Succession of toxicity and microbiota in hydraulic fracturing flowback and produced water in the Denver–Julesburg Basin. *Sci. Total Environ.* **2018**, *644*, 183–192. [[CrossRef](#)]
11. Clarkson, C.R.; Qanbari, F. An approximate semianalytical multiphase forecasting method for multifractured tight Light-Oil wells with complex fracture geometry. *J. Can. Pet. Technol.* **2015**, *54*, 489–508. [[CrossRef](#)]
12. Estrada, J.M.; Bhamidimarri, R. A review of the issues and treatment options for wastewater from shale gas extraction by hydraulic fracturing. *Fuel* **2016**, *182*, 292–303. [[CrossRef](#)]
13. Ghanbari, E.; Dehghanpour, H. The fate of fracturing water: A field and simulation study. *Fuel* **2016**, *163*, 282–294. [[CrossRef](#)]
14. Cheng, Y. Impact of water dynamics in fractures on the performance of hydraulically fractures wells in gas-shale reservoirs. *J. Can. Pet. Technol.* **2012**, *51*, 143–151. [[CrossRef](#)]
15. Zolfaghari, A.; Dehghanpour, H.; Ghanbari, E.; Bearinger, D. Fracture characterization using flowback salt-concentration transient. *SPE J.* **2016**, *21*, 233–244. [[CrossRef](#)]
16. Abbasi, M.; Dehghanpour, H.; Hawkes, R.V. Flowback analysis for fracture characterization. In Proceedings of the SPE Canadian Unconventional Resources Conference, Calgary, AL, Canada, 30 October–2 November 2012. [[CrossRef](#)]
17. King, G.E. Hydraulic Fracturing 101: What every representative, environmentalist, regulator, reporter, investor, university researcher, neighbor and engineer should know about estimating frac risk and improving frac performance in unconventional gas and oil wells. In Proceedings of the SPE Hydraulic Fracturing Technology Conference, The Woodlands, TX, USA, 6–8 February 2012. [[CrossRef](#)]
18. Perapon, F.; Torcuk, M.A.; Wallace, J.; Bertoncello, A.; Kazemi, H.; Wu, Y.-S.; Honarpour, M. Managing Shut-in Time to Enhance Gas Flow Rate in Hydraulic Fractured Shale Reservoirs: A Simulation Study. In Proceedings of the SPE Annual Technical Conference and Exhibition, New Orleans, LA, USA, 30 September–2 October 2013. [[CrossRef](#)]
19. Nicot, J.-P.; Scanlon, B.R. Water Use for Shale-Gas Production in Texas, U.S. *Environ. Sci. Technol.* **2012**, *46*, 3580–3586. [[CrossRef](#)] [[PubMed](#)]
20. Singh, H. A critical review of water uptake by shales. *J. Nat. Gas Sci. Eng.* **2016**, *34*, 751–766. [[CrossRef](#)]
21. Dehghanpour, H.; Lan, Q.; Saeed, Y.; Fei, H.; Qi, Z. Spontaneous imbibition of brine and oil in gas shales: Effect of water adsorption and resulting microfractures. *Energy Fuels* **2013**, *27*, 3039–3049. [[CrossRef](#)]
22. Roshan, H.; Ehsani, S.; Marjo, C.E.; Andersen, M.S.; Acworth, R.I. Mechanisms of water adsorption into partially saturated fractured shales: An experimental study. *Fuel* **2015**, *159*, 628–637. [[CrossRef](#)]
23. Kuru, E.; Parmar, J.S.; Dehghanpour, H. Drainage against gravity: Factors impacting the load recovery in fractures. In Proceedings of the SPE Unconventional Resources Conference—USA, The Woodlands, TX, USA, 10–12 April 2013. [[CrossRef](#)]
24. Parmar, J.; Dehghanpour, H.; Kuru, E. Displacement of water by gas in propped fractures: Combined effects of gravity, surface tension, and wettability. *J. Unconv. Oil Gas Resour.* **2014**, *5*, 10–21. [[CrossRef](#)]

25. Fan, L.; Thompson, J.W.; Robinson, J.R. Understanding gas production mechanism and effectiveness of well stimulation in the haynesville shale through reservoir simulation. In Proceedings of the Canadian Unconventional Resources and International Petroleum Conference, Calgary, AL, Canada, 19–21 October 2010. [CrossRef]
26. Xu, M.; Gupta, A.; Dehghanpour, H. How significant are strain and stress induced by water imbibition in dry gas shales? *J. Pet. Sci. Eng.* **2019**, *176*, 428–443. [CrossRef]
27. Cai, J.; Yu, B. Advances in studies of spontaneous imbibition in porous media. *Adv. Mech.* **2012**, *42*, 735–754. [CrossRef]
28. Ghanbari, E.; Dehghanpour, H. Impact of rock fabric on water imbibition and salt diffusion in gas shales. *Int. J. Coal Geol.* **2015**, *138*, 55–67. [CrossRef]
29. Muntasheri, G. A critical review of hydraulic-fracturing fluids for moderate-to ultralow-permeability formations over the last decade. *Soc. Pet. Eng. J.* **2014**, *29*, 243–260. [CrossRef]
30. Gdanski, R.; Weaver, J.; Slabaugh, B.; Walters, H.; Parker, M. Fracture face damage—It matters. In Proceedings of the European Formation Damage Conference, Sheveningen, The Netherlands, 25–27 May 2005.
31. Li, Z.; Duan, Y.; Wei, M.; Peng, Y.; Chen, Q. Pressure performance of interlaced fracture networks in shale gas reservoirs with consideration of induced fractures. *J. Pet. Sci. Eng.* **2019**, *178*, 294–310. [CrossRef]
32. Zhang, S.; Sheng, J.J. Effect of water imbibition on hydration induced fracture and permeability of shale cores. *J. Nat. Gas Sci. Eng.* **2017**, *45*, 726–737. [CrossRef]
33. Bertonecello, A.; Wallace, J.; Blyton, C.; Honarpour, M.M.; Kabir, S. Imbibition and water blockage in unconventional reservoirs: Well-management implications during flowback and early production. *SPE Reserv. Eval. Eng.* **2014**, *17*, 497–506. [CrossRef]
34. Fakcharoenphol, P.; Torcuk, M.; Kazemi, H.; Wu, Y.-S. Effect of shut-in time on gas flow rate in hydraulic fractured shale reservoirs. *J. Nat. Gas Sci. Eng.* **2016**, *32*, 109–121. [CrossRef]
35. Yuman, W.; Jinliang, H.; Xinjing, L.; Dazhong, D.; Shufang, W.; Quanzhong, G. Quantitative characterization of fractures and pores in shale beds of the Lower Silurian, Longmaxi Formation, Sichuan Basin. *Nat. Gas Ind.* **2015**, *35*, 8–15. [CrossRef]
36. Chen, Q.; Zhang, J.; Tang, X.; Li, W.; Li, Z. Relationship between pore type and pore size of marine shale: An example from the Sinian–Cambrian formation, upper Yangtze region, South China. *Int. J. Coal Geol.* **2016**, *158*, 13–28. [CrossRef]
37. Kuila, U.; Prasad, M. Specific surface area and pore-size distribution in clays and shales. *Geophys. Prospect.* **2013**, *61*, 341–362. [CrossRef]
38. He, S.G. Research of Water Imbibition Model in Shale Multiple Pores. Ph.D. Thesis, Southwest Petroleum University, Chengdu, China, 2017. Available online: http://ss.zhizhen.com/detail_38502727e7500f26321d19d4b4d28a60bfe030dee0234f581921b0a3ea255101928fa69a765a3d2d94e8dd3172203ac61d7c9cc53f22c22a2e6be98ac67925dd13f3e2a4824b8a52b564a895a5c9df8a (accessed on 1 February 2024).
39. Wang, P.Q.; Zhou, S.L. (Eds.) *Drilling Fluid and its Interaction Theory*; Petroleum Industry Press: Beijing, China, 2003.
40. Bai, M.; Green, S.; Suarez-Rivera, R. Effect of Leakoff Variation on Fracturing Efficiency for Tight Shale Gas Reservoirs. In Proceedings of the Alaska Rocks 2005, The 40th U.S. Symposium on Rock Mechanics (USRMS), Anchorage, AL, USA, 25–29 June 2005.
41. Rogers, S.; Elmo, D.; Dunphy, R.; Bearinger, D. Understanding Hydraulic Fracture Geometry and Interactions in the Horn River Basin Through DFN and Numerical Modeling. *Int. J. Sports Med.* **2010**, *31*, 458–462.
42. Rahman, M.M.; Chen, Z.; Rahman, S.S. Experimental Investigation of Shale Membrane Behavior Under Tri-Axial Condition. *Pet. Sci. Technol.* **2005**, *23*, 1265–1282. [CrossRef]

Disclaimer/Publisher’s Note: The statements, opinions and data contained in all publications are solely those of the individual author(s) and contributor(s) and not of MDPI and/or the editor(s). MDPI and/or the editor(s) disclaim responsibility for any injury to people or property resulting from any ideas, methods, instructions or products referred to in the content.